Comparison of Tumor Uptake Heterogeneity Characterization Between Static and Parametric ^{18}F-FDG PET Images in Non–Small Cell Lung Cancer

Florent Tixier[1,2], Dennis Vriens[3], Catherine Cheze-Le Rest[2,4], Mathieu Hatt[5], Jonathan A. Disselhorst[6], Wim J.G. Oyen[7], Lioe-Fee de Geus-Oei[3], Eric P. Visser[1], and Dimitris Visvikis[5]

[1]Department of Radiology, Radboud University Medical Center, Nijmegen, The Netherlands; [2]DACTIM, Medical School, University of Poitiers, Poitiers, France; [3]Department of Radiology, Leiden University Medical Centre, Leiden, The Netherlands; [4]Nuclear Medicine, CHU Poitiers, Poitiers, France; [5]INSERM, UMR 1101, LaTIM, CHU Morvan, Brest, France; [6]Department of Preclinical Imaging, Werner Siemens Imaging Center, University of Tübingen, Tübingen, Germany; and [7]Institute of Cancer Research, Royal Marsden NHS Trust, London, United Kingdom

^{18}F-FDG PET is well established in the field of oncology for diagnosis and staging purposes and is increasingly being used to assess therapeutic response and prognosis. Many quantitative indices can be used to characterize tumors on ^{18}F-FDG PET images, such as SUV$_{max}$, metabolically active tumor volume (MATV), total lesion glycolysis, and, more recently, the proposed intratumor uptake heterogeneity features. Although most PET data considered within this context concern the analysis of activity distribution using images obtained from a single static acquisition, parametric images generated from dynamic acquisitions and reflecting radiotracer kinetics may provide additional information. The purpose of this study was to quantify differences between volumetry, uptake, and heterogeneity features extracted from static and parametric PET images of non–small cell lung carcinoma (NSCLC) in order to provide insight on the potential added value of parametric images. **Methods:** Dynamic ^{18}F-FDG PET/CT was performed on 20 therapy-naive NSCLC patients for whom primary surgical resection was planned. Both static and parametric PET images were analyzed, with quantitative parameters (MATV, SUV$_{max}$, SUV$_{mean}$, heterogeneity) being extracted from the segmented tumors. Differences were investigated using Spearman rank correlation and Bland–Altman analysis. **Results:** MATV was slightly smaller on static images (−2% ± 7%), but the difference was not significant ($P = 0.14$). All derived parameters, including those characterizing tumor functional heterogeneity, correlated strongly between static and parametric images ($r = 0.70$–0.98, $P \leq 0.0006$), exhibiting differences of less than ±25%. **Conclusion:** In NSCLC primary tumors, parametric and static baseline ^{18}F-FDG PET images provided strongly correlated quantitative features for both standard (MATV, SUV$_{max}$, SUV$_{mean}$) and heterogeneity quantification. Consequently, heterogeneity quantification on parametric images does not seem to provide significant complementary information compared with static SUV images.

PET performed using ^{18}F-FDG is increasingly being applied to detect tumors, perform initial staging, monitor and plan treatment, evaluate therapeutic response, and determine prognosis (1–4). Within this context, quantitative features can be used either from baseline PET images or from a comparison between pretreatment scans and during-treatment or posttreatment scans. The SUV$_{max}$ from static images (55–65 min after injection) is the most commonly used, although it does not provide a comprehensive tumor characterization and may therefore be limited for some clinical applications (5,6). Additional standard features include SUV$_{mean}$, metabolically active tumor volume (MATV), and total lesion glycolysis (TLG, defined as MATV × SUV$_{mean}$) (7). Most ^{18}F-FDG PET–derived features are sensitive to physiologic parameters such as body composition and blood glucose concentration that may add confounding factors to inter- or intrapatient comparisons (8). Recently, PET intratumor heterogeneity characterization has been shown to have a potential added predictive and prognostic value over simple SUV measurements (9,10). However, such studies have to date been based exclusively on static PET acquisitions, which are those most commonly used in clinical practice. An alternative consists in analyzing radiotracer kinetics to provide fully quantitative information (10), such as the metabolic rate of glucose (MRGlu). Among kinetic models, Patlak analysis is considered the gold standard for modeling tissue time–activity concentration curves derived from dynamic ^{18}F-FDG PET images (11,12).

The fully quantitative parameters derived using such approaches have previously been shown to be useful in patient management (13), with differences being observed between static SUV images and parametric MRGlu images (14,15). First, SUV images reflect only the total activity, without any distinction between metabolized and unmetabolized ^{18}F-FDG uptake. In Patlak analysis, the time integral of the input time–activity curve divided by plasma concentration is plotted on the horizontal axis versus activity on the vertical axis, whereas SUV approximates this integral by

normalizing static activity concentrations using patient weight and injected dose.

Cheebsumon et al. observed different MATVs when delineated using static versus dynamic ^{18}F-FDG images (*16*), whereas Visser et al. observed that MRGlu maps led to significantly smaller MATVs than SUV-based images (*17*). The magnitude of these differences can be explained by the delineation methodology used. Threshold-based methods have been shown to lack robustness relative to varying image properties (noise, contrast) (*18*), as is the case for static PET images versus parametric PET images (*17*).

The potential interest in applying dynamic imaging to characterize intratumor heterogeneity based on texture analysis has not, to our knowledge, been evaluated. A recent review referred to the potential of features derived from parametric maps calculated using kinetic analysis in conjunction with the temporal evolution of intratumor tracer uptake distribution (*19*), without an explicit evaluation in a given patient cohort. The present study aimed to assess the potential complementary value of dynamic acquisitions and to derive quantitative parametric images for characterizing intratumor heterogeneity using ^{18}F-FDG PET. Our main objective was to quantify the potential differences between newly proposed intratumor heterogeneity characterization features from static SUV and parametric MRGlu ^{18}F-FDG PET images derived using the Patlak linearization approach (*11*). For comparison purposes, the analysis was extended to other standard PET image–derived indices such as SUV_{max}, SUV_{mean}, TLG, and MATV.

MATERIALS AND METHODS

Patients

We prospectively recruited 20 therapy-naive patients for whom primary surgical resection was planned for limited-stage non–small cell lung carcinoma (NSCLC). Tumors were required to be at least 3 cm in diameter in order to reduce the potential impact of partial-volume effects (PVE) and respiratory motion on the quantitative measurements (*20*). The study was approved by the Medical Ethics Review Committee of the Radboud University Nijmegen Medical Centre, and all patients gave written informed consent. The patient characteristics are summarized in Table 1.

^{18}F-FDG PET Acquisition and Image Reconstruction

All 20 patients underwent a dynamic PET acquisition in list mode for 60 min using a Biograph Duo scanner (Siemens Healthcare) at a single bed position (159-mm axial length) after intravenous injection of a 3.3 MBq/kg average dose using an infusion pump (an 8-mL infusion of ^{18}F-FDG at a rate of 0.2 mL/s followed by a 40-mL saline flush at a rate of 8.0 mL/s). A low-dose CT acquisition (40 mA and 130 kV) of the same area as that covered by the PET scan was used for PET attenuation correction and as an anatomic reference. The size of the CT transaxial matrix was 512×512 (0.98×0.98 mm), and the CT slice width was 3 mm.

PET data were reconstructed using a 45-frame protocol (a 10-s delay after ^{18}F-FDG injection, 16×5 s, 4×10 s, 4×20 s, 4×30 s, 4×60 s, 4×120 s, 1×150 s, and 8×300 s). Each of the 45 frames was reconstructed using 2-dimensional ordered-subsets expectation maximization in 2 dimensions with 4 iterations and 16 subsets in a $256 \times 256 \times 53$ image matrix (voxel size, $2.65 \times 2.65 \times 3.00$ mm) followed by application of an isotropic gaussian filter of 5 mm in full width at half maximum. We applied CT-based attenuation correction using a bilinear transformation of Hounsfield units to the PET energy attenuation values, a delayed-window–based randoms correction,

TABLE 1
Characteristics of the 20 Patients

Parameter	Value
Male (%)	70
Mean age (y)	63.4 (range, 44.3–77.8)
Mean body mass (kg)	78.2 (SD, 15.1)
Mean body mass index (kg/m²)	26.0 (SD, 5.3)
Mean mass activity (MBq/kg)	3.32 (SD, 0.42)*
Median serum glucose level (mmol/L)	5.3 (range, 4.5–7.7)
Location (%)	
Right upper lobe	50
Right middle lobe	5
Right lower lobe	0
Left upper lobe	35
Left lower lobe	10
Treatment (%)	
Lobectomy, R0	85
Pneumonectomy, R0	15
Histology (%)	
Squamous cell carcinoma	60
Adenocarcinoma	30
No mucinous differentiation	20
Partially mucinous	5
Mucinous differentiation	5
Sarcomatoid pleiomorph carcinoma	5
Neuroendocrine carcinoma	5
Differentiation (%)	
Poor	55
Moderate	30
Unknown	15
Mean histologic tumor diameter (mm)	52.3 (range, 15.0–85.0)†
TNM classification (%)	
T2N0M0 (stage IB)	30
T3N0M0 (stage IIB)	30
T2N1M0 (stage IIB)	40

R0 = resection margins free of tumor.

*$P = 0.193$ for 2-tailed 1-sample *t* test compared with reference mass activity of 3.45 MBq/kg.

†One lesion was smaller than 30 mm at final histology but was larger than 30 mm at CT because of surrounding organizing pneumonia.

single-scatter-simulation–based scatter correction, and decay correction. No partial volume or respiratory motion corrections were considered.

The last time frame of the dynamic series (55–60 min after injection) was used to generate the SUV images. All voxel values (Bq/mL) were normalized to the administered activity per body weight. Residual activity in the infusion system was accounted for (i.e., SUV [g/mL]).

To derive MRGlu parametric maps, MRGlu values were calculated on a voxel-by-voxel basis based on the standard 2-compartment

^{18}F-FDG model with trapping in the linear approximation (Patlak analysis) (*12*):

$$\text{MRGlu} = \frac{K_1 k_3}{k_2 + k_3}\ \frac{C_{p,glu}}{\text{LC}_{\text{FDG}}} = K_i\frac{C_{p,glu}}{\text{LC}_{\text{FDG}}},$$

where K_1, k_2, and k_3 are the 3 rate constants of the 2-compartment model, K_i (mL/g/min) is the ^{18}F-FDG influx constant, $C_{p,glu}$ is the plasma glucose concentration, and LC_{FDG} is the lumped constant (which is equal to 1). For the tissue time–activity curves, the images from frames 38–45 (i.e., 20–60 min after injection) were used, since for all tumors investigated the Patlak curves approached a straight line at 15–20 min after injection. An image-derived input function (plasma time–activity curve) was determined by considering the mean activity concentration in a manually drawn 3-dimensional volume of interest in the thoracic ascending aorta (whole blood). No plasma–to–whole-blood ratio or PVE corrections were applied. Voxelwise K_i values were subsequently determined by linear regression analysis on the Inveon Research Workplace (version 3; Siemens Healthcare) using the tissue time–activity curve and the image-derived whole-blood time–activity curve. Using the derived parametric images, we also derived for each tumor volume the metabolic rate volume (MRV = MRGlu$_{mean}$ × volume), which was used to denote the parametric equivalent of TLG in SUV images.

Image Analysis

For all patients, the primary tumor MATV was delineated on the static SUV and parametric PET images. The automatic fuzzy locally adaptive Bayesian algorithm previously validated for accuracy, robustness, and reproducibility in PET (*21,22*) was used to minimize the impact of the delineation approach on the extracted features. From these delineated volumes, the following features were extracted from both static and parametric images: MATV, maximum value (SUV$_{max}$ and K_i), metabolic volume products (TLG and MRV), and heterogeneity parameters, including the area under the curve of the cumulative intensity histogram (*23*) and textural features at both local and regional scales using previously optimized parameters (quantization into 64 levels of gray) (*24*). The area under the curve of the cumulative intensity histogram was calculated by considering all tumor voxels, consequently providing a global quantification of tumor heterogeneity. Local heterogeneity features were computed using a single cooccurrence matrix over all 13 spatial directions in 3 dimensions (*20*). These features highlight variations in intensity between contiguous voxels on the local scale and include homogeneity, entropy, and dissimilarity. Regional heterogeneity measurements were computed using matrices that link groups of intratumor voxels of similar intensity. These measurements include high-intensity emphasis and zone percentage (*24*). Most heterogeneity textural features used in this study were chosen according to previously published results regarding their reproducibility (*25*) and robustness both to functional tumor volume delineation approaches and to PVE (*18,26*).

Statistical Analysis

Statistical analysis was performed using MedCalc software. The statistics of each parameter's distribution in both images were reported using the first and third quartiles, as well as the median. The Kolmogorov–Smirnov test was used to assess the normality of distributions. Agreement between parameters from static and parametric images was assessed using the Spearman rank coefficient, and differences were quantified using Bland–Altman analysis, reporting the mean ± SD and 95% confidence intervals of the differences and the upper and lower limits (UL and LL, respectively), defined as 1.96 × SD, after application of a log transformation to parameters with a nonnormal distribution. For SUV$_{max}$ (or maximum K_i) and TLG (or MRV), only correlation coefficients are reported because the measures are not directly comparable between the two image types given the differences in units. P values of less than 0.05 were considered significant throughout the analyses.

RESULTS

Figure 1 shows examples of tumors on parametric K_i and SUV images and differences in the corresponding image indices. All features were normally distributed with the exception of MATV and TLG/MRV (Table 2). MATVs measured on static and parametric images were strongly correlated ($r = 0.96$; $P < 0.0001$; 95% confidence interval, 0.90–0.99) (Table 3). Slightly smaller MATVs were obtained on static images than on the corresponding parametric images, with nonstatistically significant differences ($-2\% \pm 7\%$; $P = 0.14$; UL/LL, $+11\%/-15\%$) (Table 3; Fig. 2A). The smallest and largest absolute volume differences were 0 and 26.5 cm^3, respectively, which were obtained for a very large tumor (>145 vs. 115 cm^3 in the parametric vs. static images).

As shown in Figure 2B, SUV$_{max}$ and maximum K_i correlated strongly ($r = 0.9$; $P < 0.0001$; 95% confidence interval, 0.76–0.99). Similarly, TLG and MRV correlated strongly, with a Spearman rank correlation coefficient of 0.98 (95% confidence interval, 0.94–0.99; $P < 0.0001$; Fig. 2C). Intratumor heterogeneity parameters for the static and parametric images also correlated ($r = 0.7$–0.91, $P \leq 0.0006$), with less than a 21% SD and UL/LL within the ±40% range, similar to
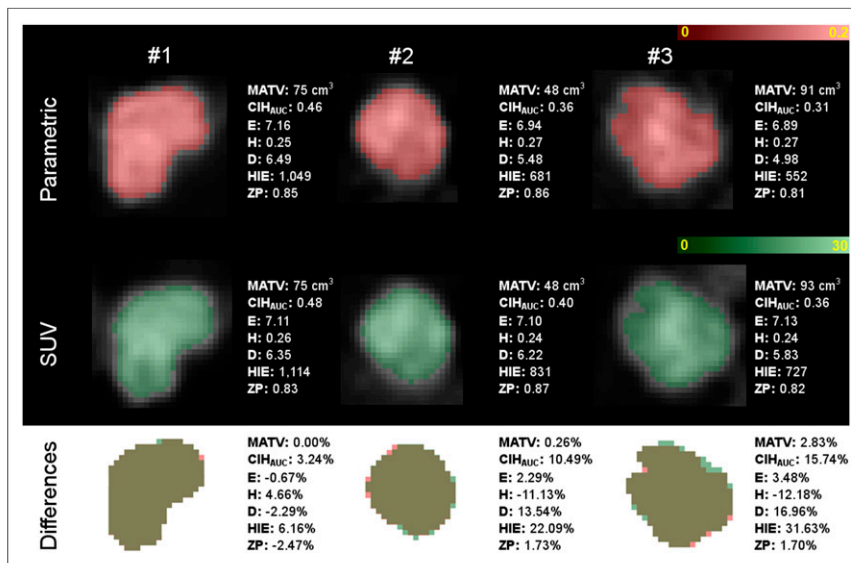
FIGURE 1. Three tumor examples, with parametric K_i and SUV images in top and middle rows, respectively, and differences between the two in bottom row. Examples 1, 2, and 3 correspond to cases with small, medium, and large differences, respectively, between parametric K_i and static SUV images. CIH$_{AUC}$ = area under curve of cumulative intensity histogram; D = dissimilarity; E = entropy; H = homogeneity; HIE = high-intensity emphasis; ZP = zone percentage.

TABLE 2
Statistics and Normality (Kolmogorov–Smirnov Test) for Features Derived from Static and Parametric ^{18}F-FDG PET Images

Parameter	Parametric				Static			
	25%	Median	75%	Normality	25%	Median	75%	Normality
MATV (cm^3)	18.43	49.51	82.47	0.01	18.83	35.39	81.29	0.006
CIH$_{AUC}$	0.27	0.30	0.35	>0.10	0.28	0.33	0.38	>0.10
Entropy	4.52	4.69	5.18	>0.10	6.46	6.72	7.08	>0.10
Homogeneity	0.51	0.55	0.56	0.0083	0.22	0.25	0.28	>0.10
Dissimilarity	2.03	2.22	2.48	>0.10	4.86	6.07	7.26	>0.10
High-intensity emphasis	854.00	1,108.00	1,229.00	>0.10	514.00	661.00	800.00	>0.10
Zone percentage	0.41	0.47	0.51	>0.10	0.82	0.86	0.88	>0.10
SUV$_{max}$/maximum K_i	0.05	0.06	0.07	0.06	9.41	12.41	14.96	>0.10
TLG/MRV	161.00	448.00	1,074.00	0.0002	1.13E+05	2.29E+05	5.14E+05	0.0001

CIH$_{AUC}$ = area under curve of cumulative intensity histogram.

the physiologic reproducibility limits previously measured on test–retest baseline PET images for such parameters (*22,25*). The heterogeneity parameters showing the lowest variability with respect to static versus parametric PET images were entropy (0.3% ± 2.1%; UL/LL, +3.8/−4.4%; Fig. 2D) and zone percentage (+1.0% ± 3.7%; UL/LL, +8.2%/−6.1%; Fig. 2E). Homogeneity led to slightly larger differences (+0.6% ± 11.9%; UL/LL, +24.0%/−22.7%), whereas dissimilarity behaved similarly to area under the curve of the cumulative intensity histogram, with SD being 16%–17% and UL/LL being about ±30%–35% (Fig. 2F). Finally, the parameter that exhibited the largest difference was high-intensity emphasis, with an SD of +0.3% ± 20.9% (UL/LL, +41.3%/−40.6%; Table 3).

DISCUSSION

There is currently increasing interest in intratumor heterogeneity characterization by PET and its potential added value for diagnosis,

evaluation of therapy response, and survival analysis. It has already been shown that, for NSCLC, the use of whole-body static ^{18}F-FDG PET to characterize intratumor heterogeneity has not only a complementary prognostic value relative to metabolic functional volume (*20,27*) but also a predictive value in the case of exclusive chemotherapy (*28*). On the other hand, there are several unanswered questions about the robustness of these heterogeneity parameters and their underlying biologic significance. Some of these parameters, including those used in this study, have been shown to be robust to physiologic reproducibility (*25,29*). In terms of their biologic significance, we have previously shown that tumor blood flow correlates strongly with various tumor heterogeneity scales extracted from ^{18}F-FDG PET images in colorectal cancer (*30*). To further evaluate the robustness of intratumor heterogeneity characterization in ^{18}F-FDG PET for NSCLC, the goal of this study was to compare, for the first time to our knowledge, intratumor heterogeneity parameters between standard static

TABLE 3
Bland–Altman and Spearman Rank Correlation Results for Comparison of Static and Parametric ^{18}F-FDG PET Images

Parameter	% difference			Bland–Altman					Spearman		
	Mean	SD	P (H0: mean = 0)	LL	95% CI for LL	UL	95% CI for UL		r	P	95% CI
MATV* (cm^3)	−2.31	6.64	0.14	−15.32	−20.72, −9.91	10.71	5.30, 16.11		0.96	<0.0001	0.90, 0.99
CIH$_{AUC}$	2.39	16.52	0.53	−29.99	−43.43, −16.55	34.77	21.33, 48.21		0.75	0.0002	0.45, 0.89
Entropy	−0.30	2.09	0.53	−4.39	−6.09, −2.69	3.80	2.10, 5.49		0.91	<0.0001	0.78, 0.96
Homogeneity	0.64	11.91	0.81	−22.71	−32.40, −13.02	23.99	14.30, 33.68		0.70	0.0006	0.38, 0.87
Dissimilarity	−1.13	16.30	0.76	−33.08	−46.34, −19.82	30.82	17.55, 44.08		0.78	<0.0001	0.52, 0.91
High-intensity emphasis	0.32	20.89	0.95	−40.63	−57.63, −23.63	41.27	24.27, 58.26		0.77	0.0001	0.51, 0.91
Zone percentage	1.04	3.65	0.22	−6.11	−9.07, −3.14	8.18	5.22, 11.15		0.74	0.0002	0.44, 0.89
SUV$_{max}$/maximum K_i	—	—	—	—	—	—	—		0.90	<0.0001	0.76, 0.96
TLG/MRV*	—	—	—	—	—	—	—		0.98	<0.0001	0.94, 0.99

*TLG/MRV and MATV were log-transformed.
H$_0$ = the null hypothesis; CI = confidence interval; CIH$_{AUC}$ = area under curve of cumulative intensity histogram.
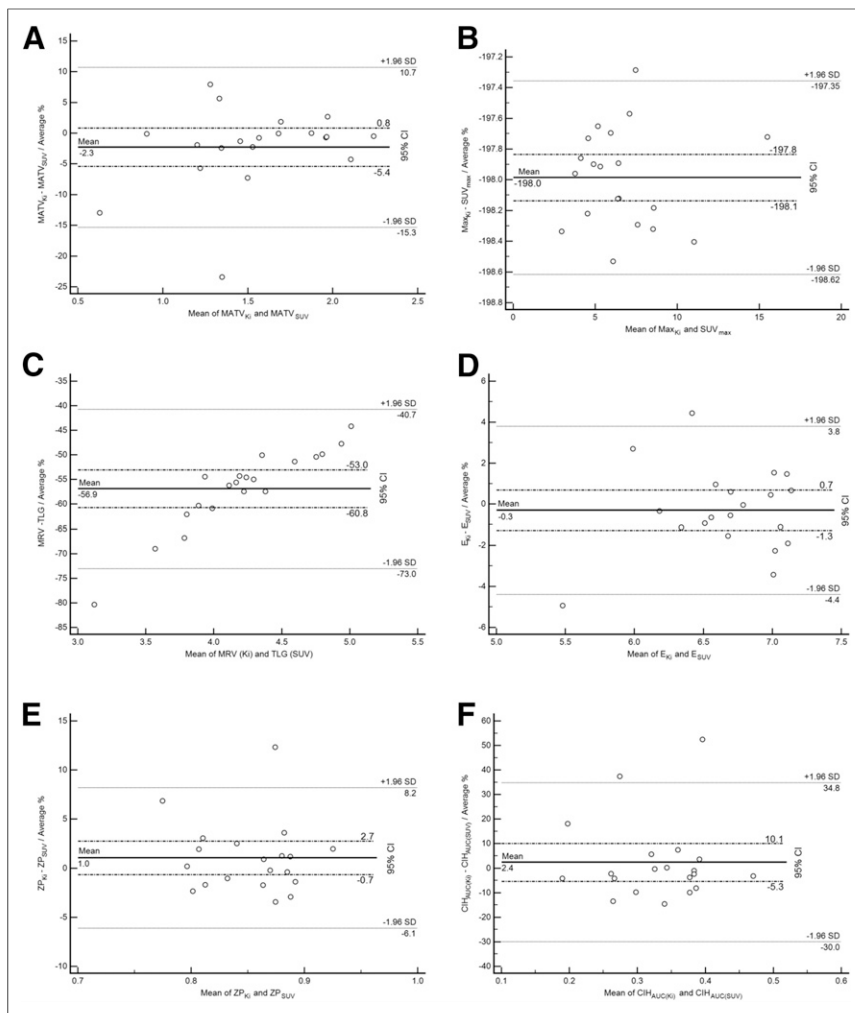
FIGURE 2. Bland–Altman plot of MATV (logarithmic transformation) (A), area under curve of cumulative intensity histogram (B), SUV_{max}/maximum K_i (C), TLG/MRV (logarithmic transformation) (D), entropy (E), and zone percentage (F). Each graph reports mean ± 1.96 SD and 95% confidence interval for mean of differences. AUC = area under curve; CIH = cumulative intensity histogram; E = entropy; ZP = zone percentage.

We also found that measurement of maximum intensity (SUV_{max} and maximum K_i) and total activity (TLG and MRV) correlated strongly between static and parametric images ($r \geq 0.9$). This observation is in line with results previously reported for renal cell carcinoma metastases by Freedman et al. (14) and for breast cancer by Doot et al. (33). Both found a strong correlation ($r > 0.95$) between SUV_{max} and maximum K_i on baseline ^{18}F-FDG PET scans.

Most of the uptake heterogeneity features considered in the present study correlated strongly ($r \geq 0.7$, $P \leq 0.0006$) when obtained using static or parametric PET images, with differences of less than ±25%, except for high-intensity emphasis (±40%) and dissimilarity (±30%). In particular, entropy and zone percentage values were quite similar (<±5% and <±9%, respectively), providing further evidence of the robustness of these parameters in characterizing intratumor heterogeneity (18,26). The strongest differences associated with high-intensity emphasis may be explained by its previously demonstrated lower robustness to PVE (mean difference of −20.6 ± 18.8 between PVE-corrected and non–PVE-corrected images) (18).

In comparisons of quantitative measurements of intratumor heterogeneity between static and parametric ^{18}F-FDG images, our results suggest that the observed differences, rather than representing the actual spatial distribution of uptake, can be attributed mostly to variability in image characteristics and noise (Fig. 1). This possibility, in turn, supports the hypothesis that with respect to intratumor heterogeneity characterization the parametric images provide information similar to that of static SUV images on a ^{18}F-FDG PET baseline scan.

On the basis of the Patlak analysis assumptions and use of the baseline scan only, the hypotheses of this work were that the unmetabolized component of ^{18}F-FDG is negligible at later times and that the ratio of injected dose to patient weight is proportional to the area under the curve of the arterial input function. If one considers a comparison of a baseline scan and an early or late scan, such as in early–late therapy response monitoring, the conclusions may be different. Although such an analysis was beyond the objectives of this work, in such a comparative framework parametric images may eventually provide useful additional information. For example, it has previously been demonstrated—within the context of early prediction of the response of locally advanced breast cancer to therapy—that dynamic PET scans provide clinical added value to static SUV measurements, leading to significantly higher predictive accuracy (34). That study, however, was based on comparison of SUV measurements only and did

acquisitions and quantitative parametric ^{18}F-FDG PET images. The underlying goal of this comparison was to provide some insight into the potential information that parametric images may add to that obtained from standard clinical PET acquisitions.

First, the use of a robust delineation approach allowed us to overcome the potential robustness issues previously observed (21) in the determination of MATVs measured from static versus parametric PET images (−2% ± 7% and limits of 11%–15%). The observed variations, at ±30%, were well within the upper and lower physiologic reproducibility limits previously determined for the fuzzy locally adaptive Bayesian approach (22) and substantially lower than those previously reported using less robust delineation methods based on fixed thresholding (17). Fixed thresholding has been shown to lack robustness and to be sensitive to tumor contrast (31). The higher contrast in parametric images (32) may explain MATV differences that were not observed in the present study using a more robust delineation algorithm.

not include more advanced tumor characterization metrics (volume, heterogeneity).

Our study was limited by the small number of patients and the exclusion of NSCLC patients with large lesions (>3 cm). Despite the few patients, the small mean differences in parameters suggest that similar information on tumor heterogeneity can be derived from the static and parametric baseline ^{18}F-FDG PET images. Given these small differences, a more substantial patient cohort is needed to confirm the statistical significance of these results. We chose to limit lesion size in order to reduce the influence of both respiratory motion and PVE. Although previous studies have shown variability in heterogeneity features as a result of respiratory gating (35,36), other studies have shown no statistically significant differences in the PET heterogeneity parameters considered in the present study (37). In addition, most of the lesions in our study (85%) were in the upper lung lobes, which are less influenced by respiratory motion.

The choice of NSCLC as the cancer type in our study can also be a limitation because lung tissue is mostly metabolically nonactive and thus the background is low and the fraction of unmetabolized ^{18}F-FDG is also low. Our present conclusions for NSCLC therefore cannot be extended to tumors in tissues with higher background levels (e.g., liver metastases) or near reservoirs of metabolically inactive ^{18}F-FDG, such as in urine or even blood (especially in end-stage renal failure).

Although the strong correlation between features extracted from static and parametric PET images suggests that there is no significant complementary information to be derived from parametric ^{18}F-FDG PET images, further validation studies are required to compare the actual predictive and prognostic value of static versus parametric images for patient response and overall survival in NSCLC.

CONCLUSION

In NSCLC, parametric and static SUV ^{18}F-FDG PET images provided similar and strongly correlated findings for tumor-derived characterization parameters. More specifically, similar correlations and small differences were found for such metrics as entropy and zone percentage, which quantify heterogeneity in the spatial distribution of intratumor uptake. Despite the limited number of patients and the lack of correction for respiratory motion, our findings suggest that within the context of NSCLC patient management, dynamic ^{18}F-FDG PET has no added value over a single baseline ^{18}F-FDG PET image in the analysis of intratumor heterogeneity.

DISCLOSURE

REFERENCES

1. Czernin J, Benz MR, Allen-Auerbach MS. PET/CT imaging: the incremental value of assessing the glucose metabolic phenotype and the structure of cancers in a single examination. *Eur J Radiol.* 2010;73:470–480.

2. Grégoire V, Haustermans K, Geets X, Roels S, Lonneux M. PET-based treatment planning in radiotherapy: a new standard? *J Nucl Med.* 2007;48(suppl 1):68S–77S.

3. Harry VN, Semple SI, Parkin DE, Gilbert FJ. Use of new imaging techniques to predict tumour response to therapy. *Lancet Oncol.* 2010;11:92–102.

4. Jadvar H, Alavi A, Gambhir SS. ^{18}F-FDG uptake in lung, breast, and colon cancers: molecular biology correlates and disease characterization. *J Nucl Med.* 2009;50:1820–1827.

5. Hatt M, Visvikis D, Pradier O, Cheze-le Rest C. Baseline ^{18}F-FDG PET image-derived parameters for therapy response prediction in oesophageal cancer. *Eur J Nucl Med Mol Imaging.* 2011;38:1595–1606.

6. Wieder HA, Ott K, Lordick F, et al. Prediction of tumor response by FDG-PET: comparison of the accuracy of single and sequential studies in patients with adenocarcinomas of the esophagogastric junction. *Eur J Nucl Med Mol Imaging.* 2007;34:1925–1932.

7. Larson SM, Erdi Y, Akhurst T, et al. Tumor treatment response based on visual and quantitative changes in global tumor glycolysis using PET-FDG imaging. the visual response score and the change in total lesion glycolysis. *Clin Positron Imaging.* 1999;2:159–171.

8. Boellaard R. Standards for PET image acquisition and quantitative data analysis. *J Nucl Med.* 2009;50(suppl 1):11S–20S.

9. Rizk NP, Tang L, Adusumilli PS, et al. Predictive value of initial PET-SUVmax in patients with locally advanced esophageal and gastroesophageal junction adenocarcinoma. *J Thorac Oncol.* 2009;4:875–879.

10. Hoekstra CJ, Paglianiti I, Hoekstra OS, et al. Monitoring response to therapy in cancer using [^{18}F]-2-fluoro-2-deoxy-D-glucose and positron emission tomography: an overview of different analytical methods. *Eur J Nucl Med.* 2000;27:731–743.

11. Vriens D, Visser EP, de Geus-Oei LF, Oyen WJ. Methodological considerations in quantification of oncological FDG PET studies. *Eur J Nucl Med Mol Imaging.* 2010;37:1408–1425.

12. Patlak CS, Blasberg RG, Fenstermacher JD. Graphical evaluation of blood-to-brain transfer constants from multiple-time uptake data. *J Cereb Blood Flow Metab.* 1983;3:1–7.

13. Cheebsumon P, Velasquez LM, Hoekstra CJ, et al. Measuring response to therapy using FDG PET: semi-quantitative and full kinetic analysis. *Eur J Nucl Med Mol Imaging.* 2011;38:832–842.

14. Freedman NM, Sundaram SK, Kurdziel K, et al. Comparison of SUV and Patlak slope for monitoring of cancer therapy using serial PET scans. *Eur J Nucl Med Mol Imaging.* 2003;30:46–53.

15. Weber WA. Use of PET for monitoring cancer therapy and for predicting outcome. *J Nucl Med.* 2005;46:983–995.

16. Cheebsumon P, van Velden FH, Yaqub M, et al. Measurement of metabolic tumor volume: static versus dynamic FDG scans. *EJNMMI Res.* 2011;1:35.

17. Visser EP, Philippens ME, Kienhorst L, et al. Comparison of tumor volumes derived from glucose metabolic rate maps and SUV maps in dynamic ^{18}F-FDG PET. *J Nucl Med.* 2008;49:892–898.

18. Hatt M, Tixier F, Cheze Le Rest C, Pradier O, Visvikis D. Robustness of intratumour ^{18}F-FDG PET uptake heterogeneity quantification for therapy response prediction in oesophageal carcinoma. *Eur J Nucl Med Mol Imaging.* 2013;40:1662–1671.

19. El Naqa I. The role of quantitative PET in predicting cancer treatment outcomes. *Clin Transl Imaging.* 2014;2:305–320.

20. Hatt M, Majdoub M, Vallieres M, et al. ^{18}F-FDG PET uptake characterization through texture analysis: investigating the complementary nature of heterogeneity and functional tumor volume in a multi-cancer site patient cohort. *J Nucl Med.* 2015;56:38–44.

21. Hatt M, Cheze Le Rest C, Albarghach N, Pradier O, Visvikis D. PET functional volume delineation: a robustness and repeatability study. *Eur J Nucl Med Mol Imaging.* 2011;38:663–672.

22. Hatt M, Cheze-Le Rest C, Aboagye EO, et al. Reproducibility of ^{18}F-FDG and 3′-deoxy-3′-^{18}F-fluorothymidine PET tumor volume measurements. *J Nucl Med.* 2010;51:1368–1376.

23. van Velden FH, Cheebsumon P, Yaqub M, et al. Evaluation of a cumulative SUV-volume histogram method for parameterizing heterogeneous intratumoural FDG uptake in non-small cell lung cancer PET studies. *Eur J Nucl Med Mol Imaging.* 2011;38:1636–1647.

24. Tixier F, Le Rest CC, Hatt M, et al. Intratumor heterogeneity characterized by textural features on baseline ^{18}F-FDG PET images predicts response to concomitant radiochemotherapy in esophageal cancer. *J Nucl Med.* 2011;52:369–378.

25. Tixier F, Hatt M, Le Rest CC, Le Pogam A, Corcos L, Visvikis D. Reproducibility of tumor uptake heterogeneity characterization through

textural feature analysis in ^{18}F-FDG PET. *J Nucl Med.* 2012;53:693–700.

26. Galavis PE, Hollensen C, Jallow N, Paliwal B, Jeraj R. Variability of textural features in FDG PET images due to different acquisition modes and reconstruction parameters. *Acta Oncol.* 2010;49:1012–1016.

27. Tixier F, Hatt M, Valla C, et al. Visual versus quantitative assessment of intratumor ^{18}F-FDG PET uptake heterogeneity: prognostic value in non-small cell lung cancer. *J Nucl Med.* 2014;55:1235–1241.

28. Cook GJ, O'Brien ME, Siddique M, et al. Non-small cell lung cancer treated with erlotinib: heterogeneity of F-FDG uptake at PET—association with treatment response and prognosis. *Radiology.* 2015;276:883–893.

29. Willaime JM, Turkheimer FE, Kenny LM, Aboagye EO. Quantification of intra-tumour cell proliferation heterogeneity using imaging descriptors of ^{18}F fluorothymidine-positron emission tomography. *Phys Med Biol.* 2013;58:187–203.

30. Tixier F, Groves AM, Goh V, et al. Correlation of intra-tumor ^{18}F-FDG uptake heterogeneity indices with perfusion CT derived parameters in colorectal cancer. *PLoS One.* 2014;9:e99567.

31. Hatt M, Cheze le Rest C, Turzo A, Roux C, Visvikis D. A fuzzy locally adaptive Bayesian segmentation approach for volume determination in PET. *IEEE Trans Med Imaging.* 2009;28:881–893.

32. Sayre GA, Franc BL, Seo Y. Patient-specific method of generating parametric maps of Patlak K(i) without blood sampling or metabolite correction: a feasibility study. *Int J Mol Imaging.* 2011;2011:1–12.

33. Doot RK, Dunnwald LK, Schubert EK, et al. Dynamic and static approaches to quantifying ^{18}F-FDG uptake for measuring cancer response to therapy, including the effect of granulocyte CSF. *J Nucl Med.* 2007;48:920–925.

34. Dunnwald LK, Doot RK, Specht JM, et al. PET tumor metabolism in locally advanced breast cancer patients undergoing neoadjuvant chemotherapy: value of static versus kinetic measures of fluorodeoxyglucose uptake. *Clin Cancer Res.* 2011;17:2400–2409.

35. Vaidya M, Creach KM, Frye J, Dehdashti F, Bradley JD, El Naqa I. Combined PET/CT image characteristics for radiotherapy tumor response in lung cancer. *Radiother Oncol.* 2012;102:239–245.

36. Yip S, McCall K, Aristophanous M, Chen AB, Aerts HJ, Berbeco R. Comparison of texture features derived from static and respiratory-gated PET images in non-small cell lung cancer. *PLoS One.* 2014;9:e115510.

37. Grootjans W, Tixier F, van der Vox S, et al. Impact of optimal respiratory gated positron emission tomography on characterisation of intra-tumour heterogeneity in lung cancer patients. *Eur J Nucl Med Mol Imaging.* 2015;42(suppl 1):S640.